Metallic Transport in a Monatomic Layer of In on a Silicon Surface

Shiro Yamazaki,[1,*] Yoshikazu Hosomura,[1] Iwao Matsuda,[2] Rei Hobara,[1] Toyoaki Eguchi,[2] Yukio Hasegawa,[2] and Shuji Hasegawa[1]

[1]*Department of Physics, School of Science, The University of Tokyo, 7-3-1 Hongo, Bunkyo-ku, Tokyo 113-0033, Japan*

[2]*The Institute for Solid State Physics, The University of Tokyo, 5-1-5 Kashiwa-no-ha, Kashiwa, 277-8581, Japan*

(Received 3 February 2009; revised manuscript received 13 November 2010; published 14 March 2011)

We have succeeded in detecting metallic transport in a monatomic layer of In on an Si(111) surface, Si(111) $-\sqrt{7}\times\sqrt{3}$-In surface reconstruction, using the micro-four-point probe method. The In layer exhibited conductivity higher than the minimum metallic conductivity (the Ioffe-Regel criterion) and kept the metallic temperature dependence of resistivity down to 10 K. This is the first example of a monatomic layer, with the exception of graphene, showing metallic transport without carrier localization at cryogenic temperatures. By introducing defects on this surface, a metal-insulator transition occurred due to Anderson localization, showing hopping conduction.

DOI: 10.1103/PhysRevLett.106.116802 PACS numbers: 73.20.−r, 73.25.+i, 73.63.−b

Metallic transport, which means conductivity higher than the minimum metallic conductivity and a decrease in resistivity by cooling, is an old but still new issue in condensed matter physics, especially at nanometer scales. Since electrical transport in nanoscale low-dimensional systems is affected by atomic disorder and defects much more than in three-dimensional bulk materials, it has been thought that it is difficult for such low-dimensional systems to exhibit metallic transport at low temperatures due to defect-induced Anderson localization [1,2]. However, in recent years, atomic-scale low-dimensional systems showing metallic transport even at low temperatures have been found, such as high-quality polyaniline one-dimensional (1D) molecular chains [3] and graphene, a monatomic layer of carbon [4,5].

Here, we report a transport study on an indium monatomic layer deposited on a Si(111) surface, Si(111) $-\sqrt{7}\times\sqrt{3}$-In surface reconstruction, by using the micro-four-point probe (μ4PP) method [6,7]. It was found for the first time that with the exception of graphene, the monatomic layer showed a higher conductivity than the minimum metallic conductivity as well as metallic temperature dependence of resistivity. Furthermore, by intentionally introducing defects on the surface, the resistivity increased dramatically and a metal-insulator transition occurred due to Anderson localization.

By depositing In on the Si(111) surface, various kinds of surface reconstructions are formed [8]. The $\sqrt{3}\times\sqrt{3}$ [Figs. 1(a) and 1(b)] and the $\sqrt{31}\times\sqrt{31}$ surfaces [Figs. 1(c) and 1(d)] are insulating with a band gap of $\sim$1 eV at the Fermi level [9]. The 4×1 surface [Figs. 1(e) and 1(f)] exhibits a quasi-1D metallic band structure [10]. Because of its Peierls instability at low temperatures, this surface exhibits a metal-to-insulator transition upon cooling [11]. The $\sqrt{7}\times\sqrt{3}$ surface [Figs. 1(g) and 1(h)] exhibits a circular Fermi surface and a parabolic band dispersion as revealed by photoemission spectroscopy (PES), suggesting a free-electron-like two-dimensional (2D) metallic system [12]. The evaluated effective mass m^* and Fermi wave number k_F are $1.1m_e$ (m_e; electron's rest mass) and 14 nm^{-1}, respectively. k_F is quite large compared to the values for typical metallic surfaces such as Si(111) $-\sqrt{3}\times\sqrt{3}$-Ag (0.8 nm^{-1}) and -Au (1.5 nm^{-1}) [13]. This fact is crucial to yield low surface resistivity and metallic transport. The structure of the $\sqrt{7}\times\sqrt{3}$ surface is

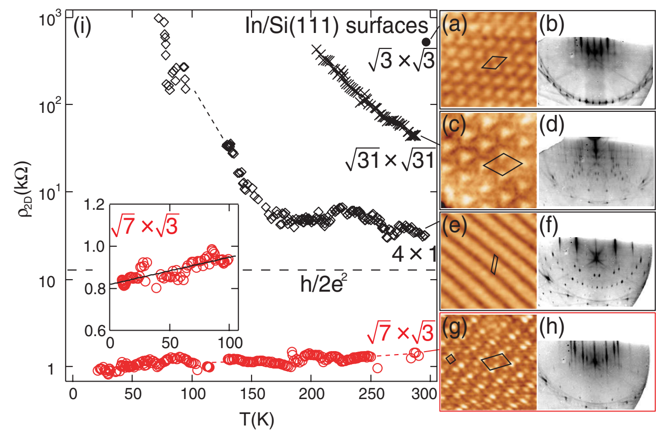

FIG. 1 (color online). (a)(b), (c)(d), (e)(f), and (g)(h) are STM images and RHEED patterns of the $\sqrt{3}\times\sqrt{3}$ ($V_{(\mathrm{Sample})} = 1.6$ V, size:5 nm), the $\sqrt{31}\times\sqrt{31}$ ($V = 1.9$ V, 10 nm), the 4×1($V = -1.0$ V, 10 nm), and the $\sqrt{7}\times\sqrt{3}$ ($V = -0.0091$ V, 5 nm) surfaces, respectively. The unit cell of each surface is indicated in the image. [The In(001) $-(1\times1)_{\mathrm{rect}}$ unit cell is also indicated in (g).] (i) Measured sheet resistivities (ρ_{2D}) plotted on a logarithmic scale as a function of temperature for the In/Si(111) surfaces: the $\sqrt{3}\times\sqrt{3}$ (filled circles), $\sqrt{31}\times\sqrt{31}$ (crosses), 4×1 (diamonds), and $\sqrt{7}\times\sqrt{3}$ (open circles). The horizontal broken line indicates the inverse of the minimum metallic conductivity. The inset shows the measured sheet resistivity for the $\sqrt{7}\times\sqrt{3}$ surface at low temperatures. The STM images and resistivity data were obtained in different UHV systems, both of which were equipped with RHEED.

 © 2011 American Physical Society

approximately understood to be a monatomic layer of In (001) having quasi-fourfold symmetry [9]. The unit cell (0.866×0.833 Å^2) based on the rectangular lattice is also shown in Fig. 1(g).

The resistivity was measured *in situ* using a μ4PP chip with a probe spacing of 20 μm [6], at temperatures (T) ranging from room temperature (RT) to 10 K, in an ultrahigh-vacuum (UHV) chamber [7]. The applied force to the μ4PP chip was 10–100 nN [6,7]. The damaged area at the probe contact was several nm^2, which was negligible comparing with the probe spacing (20 μm). Scanning tunneling microscope (STM) images were recorded with a customized STM based on a commercial STM (JEOL) in a separate UHV chamber. Both UHV chambers were equipped with reflection-high-energy electron diffraction (RHEED) to confirm common preparation of samples. The Si(111) substrate was an n-type (P-doped) with 1–10 Ω cm resistivity at RT. Indium was deposited on a clean Si(111)-(7×7) reconstructed surface kept at appropriate annealing temperatures. The In coverage and annealing temperature used for the respective In/Si(111) surface were (0.33 ML, 500 °C) for the $\sqrt{3} \times \sqrt{3}$ surface, (0.50 ML, 450 °C) for the $\sqrt{31} \times \sqrt{31}$ surface, and (1.0 ML, 450 °C) for the 4×1 surface. The deposition rate was calibrated using the phase diagram of the In/Si (111) system [14]. About 1.7 ML In was first deposited on the 7×7 surface at RT and flash heated at 500 °C to fabricate the $\sqrt{7} \times \sqrt{3}$ surface [12]. In this process, excess In atoms are desorbed from the sample, resulting in the formation of the $\sqrt{7} \times \sqrt{3}$ surface which ideally has 1.2 ML In coverage. Longer heating for a few seconds caused the formation of the 4×1 surface by further desorbing In atoms.

We estimated the conductivity of the surface-space-charge layer of the respective In/Si(111) surfaces by solving the Poisson equation with parameters derived from the reported band bending [15–18]. This conductivity was found to be negligibly small compared to the measured conductivity. Furthermore, the band bending indicates that a pn junction is formed between the surface-space charge layer (p-type) and the underlying bulk (n-type), which prevents the measuring current from penetrating into the substrate bulk. In addition, the temperature dependence of the measured resistivity of the $\sqrt{7} \times \sqrt{3}$ surface was completely different from that of the surface-space-charge layer and the bulk Si crystal at low temperatures. Therefore, we can state that the measured conductivity was dominated by the surface states.

Figure 1(i) shows the sheet resistivities ρ_{2D}, which were obtained from the measured 4PP resistance R by $\rho_{2D} = (\pi R)/\ln 2$, plotted on a logarithmic scale as a function of temperature for all surfaces. The values of resistivity and its temperature dependences significantly depend on the surface. The resistivities of the semiconducting ones, the $\sqrt{31} \times \sqrt{31}$ surface and the $\sqrt{3} \times \sqrt{3}$ surface, are much larger than the inverse of the minimum metallic conductivity (quantum resistivity: $h/2e^2 = 12.9$ kΩ) and increase with cooling (semiconducting temperature dependence). The activation energy evaluated from the temperature dependence of the $\sqrt{31} \times \sqrt{31}$ surface is about 0.2 eV, which is smaller than the reported band gap $\sim$1 eV [9]. A metal-insulator transition by Peierls instability has been reported on a 4×1 surface [19]. Our 4×1 surface shows a semiconducting temperature dependence at the high-temperature phase because the resistivity is higher than the inverse of the minimum metallic conductivity probably due to defects. An abrupt change in the temperature dependence at 150 K is indicative of the metal-to-insulator transition.

Figure 1(i) and the inset show sheet resistivities of the $\sqrt{7} \times \sqrt{3}$ surface recorded with decreasing and increasing temperature, respectively. Both resistivities showed the same temperature dependence irrespective of the temperature ramping direction, demonstrating the reliability of our measurements. The resistivity of the $\sqrt{7} \times \sqrt{3}$ surface is much lower than the inverse of the minimum metallic conductivity, and monotonically decreased with cooling (metallic temperature dependence) from RT to 10 K. In other words, this surface satisfies the Ioffe-Regel criterion, which is needed for metallic conduction [20]. The inset in Fig. 1(i) shows a linear-scale plot below 100 K. The solid line is the fitting result by the metallic temperature dependence:

$$\rho_{2D} = \frac{4\pi^2 m^* \lambda}{\hbar e^2 k_F^2} k_B T + \rho_0. \quad (1)$$

This equation is derived from the 2D Boltzmann equation, $\rho_{2D} = (2\pi m^*)/(e^2 k_F^2 \tau_{in})$. Temperature dependence of the phonon-induced inelastic relaxation time $\tau_{in} = \hbar/(2\pi\lambda k_B T)$ is derived using Debye approximation at temperature higher than Debye temperature [21,22], where k_B is the Boltzmann constant. Here umklapp processes are neglected. Our fitting result gives an electron-phonon coupling constant of $\lambda = 1.2$ and residual sheet resistivity of $\rho_0 = 820$ Ω. This value of λ is large, but consistent with the value estimated by PES, $\lambda \sim 1$ [12]. In general, the λ value is typically 0.1–0.3 for bulk metals, while it tends to be large at surfaces, and exceeds unity in some surfaces [22]. The residual resistivity ratio [RRR $\equiv \rho(\mathrm{RT})/\rho(4K) \approx \rho(\mathrm{RT})/\rho_0$] is found to be 1.3, which is smaller by 2 orders of magnitude than the RRR of typical bulk metals. This means that in such atomic-scale low-dimensional systems, carrier scattering by defects contributes significantly to the resistivity. The evaluated average relaxation time (τ) (0.92 fs at RT, 1.3 fs at 10 K) and mean free path ($\ell = v_F \tau$) (1.4 nm at RT, 1.9 nm at 10 K) do not change as much upon cooling. This leads to $k_F \ell = 20$–30, which is much larger than unity, ensuring the Ioffe-Regel criterion [20]. The mean free path $\sim$2 nm is slightly shorter than the roughly estimated point defect separation

~10 nm in STM images. The deviation may be due to line defects such as steps and domain boundaries that scatter electrons more strongly. Recently, the $\sqrt{7}\times\sqrt{3}$ surface has been reported to be the first one-atomic layer exhibiting possible superconductivity at $T < 3.18$ K, by scanning tunneling spectroscopy measurements [23]. Therefore a transport measurement at lower temperatures is highly desired.

Figure 2(a) shows the measured sheet resistivities as a function of temperature for several surfaces with different densities of defects. Defects were observed by wide-view STM images [Figs. 2(b), 2(d), and 2(f)] and *in situ* RHEED patterns around the 0th Laue zone [Figs. 2(c), 2(e), and 2(g)]. As shown in Fig. 1(i) and also in Fig. 2(a), the pristine $\sqrt{7}\times\sqrt{3}$ surface shows metallic transport. The STM image exhibits a small number of dark spots with a defect density of 0.004 nm^{-2}. However, the 100L-O_2 exposed $\sqrt{7}\times\sqrt{3}$ surface shows higher resistivities and a semiconducting temperature dependence (circled crosses), following a thermal activation-type function with a small activation energy $\Delta E = 1.0$ meV. The STM image exhibited additional bright spots indicated by the black arrow in Fig. 2(d). The defect density was roughly 0.03 nm^{-2}. The RHEED pattern shows weaker superlattice spots [Fig. 2(e)]. A surface fabricated by 2 ML In deposition on a Si(111)-(7 × 7) surface at RT without postannealing exhibits a larger resistivity (triangles) even though the surface has In coverage nearly 2 times greater than the $\sqrt{7}\times\sqrt{3}$ surface. The STM image shows a granular In film partially connected to each other [Fig. 2(b)]. The defect density is roughly 0.3–0.5 nm^{-2}. The RHEED pattern shows no spots except for the specular reflection [Fig. 2(c)]. The temperature dependence of the resistivity is thermal activation type with an activation energy of $\Delta E = 32$ meV. The conduction mechanism is thought to be hopping conduction between granular islands. One of the other samples of $\sqrt{7}\times\sqrt{3}$ surface, which showed a slightly weak $\sqrt{7}\times\sqrt{3}$ RHEED spots, exhibited a semiconducting temperature dependence as shown by downward triangles in Fig. 2(a). The critical resistivity dividing the metallic T dependence from the insulating one is about 3 kΩ in this case. This value is several times smaller than the inverse of the minimum metallic conductivity. These results clearly show that the resistivity is significantly increased by introducing small amounts of defects, and the temperature dependence also changes drastically. Therefore, forming a high-quality surface is crucial for obtaining metallic transport.

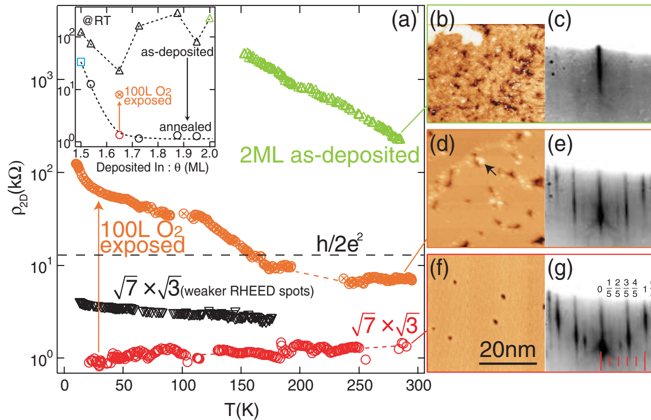

FIG. 2 (color online). (a) Measured sheet resistivity (ρ_{2D}) as a function of temperature for the pristine $\sqrt{7}\times\sqrt{3}$ surface (circles), the $\sqrt{7}\times\sqrt{3}$ (weaker RHEED spots) surface (downward triangles), the 100L-O_2 exposed $\sqrt{7}\times\sqrt{3}$ surface (circled crosses), and the 2 ML-In as-deposited surface (triangles). The inset shows the measured sheet resistivities at RT as a function of the amount of deposited In for the as-deposited surfaces (triangles) and annealed surfaces (circles and square). (b)(c), (d)(e), and (f)(g) are wide-view STM images and RHEED patterns of the 0th Laue rings of the 2 ML as-deposited surface ($V = 1.6$ V), with the 100L-O_2 exposed $\sqrt{7}\times\sqrt{3}$ surface ($V = 1.9$ V) and the pristine $\sqrt{7}\times\sqrt{3}$ surface ($V = -1.19$ V), respectively. The common scale is shown in (f). The superlattice spots are indicated by fractional numbers and lines in (g).

The inset in Fig. 2(a) shows the sheet resistivity at RT as a function of the amount of deposited In. For surfaces without postannealing (as deposited), the resistivity does not vary systematically with the amount of deposited In (triangles). This means that additional In does not contribute to the electrical conduction due to poor connections between the In islands. The high-temperature flash heating (500 °C) causes the formation of the $\sqrt{7}\times\sqrt{3}$ surface, resulting in a drastic decrease in resistivity. The resistivity of the $\sqrt{7}\times\sqrt{3}$ surface decreased with increasing amount of deposited In from 1.5 to 1.6 ML. However, with more than 1.6 ML, it becomes constant around 1 kΩ. This suggests that more than 1.6 ML, the $\sqrt{7}\times\sqrt{3}$ surface, which ideally has 1.2 ML In, is fabricated completely by the heating procedure. However, with less than 1.6 ML, the formed $\sqrt{7}\times\sqrt{3}$ surface is defective.

Figure 3(a) shows the log-scale sheet resistivity as a function of the temperature below 50 K for the defective $\sqrt{7}\times\sqrt{3}$ surface prepared with 1.5 ML In deposition (the defective $\sqrt{7}\times\sqrt{3}$ surface hereafter). The inset in Fig. 3(a) shows the STM image with a slightly higher defect density of 0.009 nm^{-2} than the pristine case where the defect density is 0.004 nm^{-2}. Unlike the pristine $\sqrt{7}\times\sqrt{3}$ surface showing the metallic temperature dependence, the defective $\sqrt{7}\times\sqrt{3}$ surface shows a semiconducting temperature dependence. Three functions based on different theories are used for fitting the data. The solid line in Fig. 3(b) is the fitting using the Anderson weak localization theory for a 2D metal [1,24], $\sigma_{2D} = \alpha(e^2/2\pi^2 h)\ln T + C$. The evaluated fitting parameters are $\alpha = 0.0471$ and $C = -0.257$. The physical meaning of α is the power related to the temperature dependence of the phase relaxation time of the carriers ($\tau_\phi \propto T^{-\alpha}$). The range of α needs to be between 1 and 2. Since the evaluated value of α is

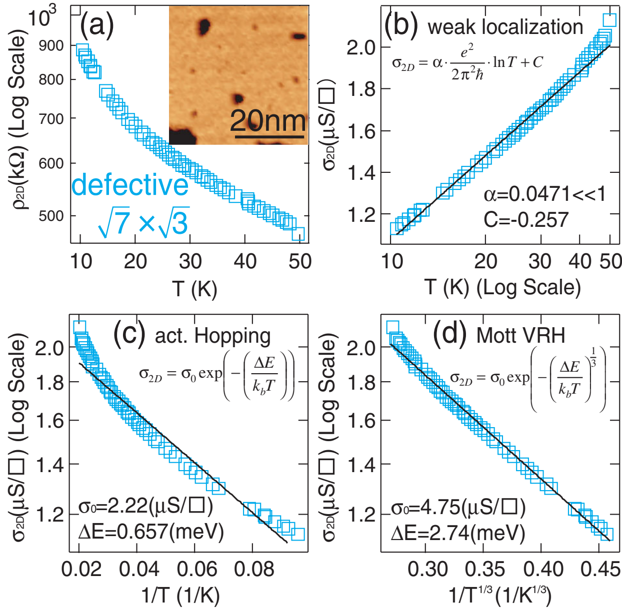

FIG. 3 (color online). (a) Measured sheet resistivities (ρ_{2D}) plotted on a logarithmic scale as a function of temperature ranging from 50 to 10 K for the defective $\sqrt{7}\times\sqrt{3}$ surface. (b)(c)(d) Sheet conductivities σ_{2D} for the same data as in (a); (b) plotted as a function of T (on a logarithmic scale), (c) plotted on a logarithmic scale as a function of the inverse of T, (d) plotted on a logarithmic scale as a function of $1/T^{1/3}$. In (b), (c), and (d), the solid lines indicate the fitting results by the functions with parameters displayed in each figure. The inset in (a) shows the STM image ($V = -1.77$ V).

much smaller than unity, the weak localization picture does not work in this case. The solid line in Fig. 3(c) is the fitting result using the conventional semiconducting temperature dependence, $\sigma_{2D} = \sigma_0 \exp(-\Delta E/k_B T)$ with fitting parameters $\sigma_0 = 2.22\ \mu S/\square$ and $\Delta E = 0.657$ meV. However, the best fitted solid line does not reproduce the experimental results well. This means that the defective $\sqrt{7}\times\sqrt{3}$ surface does not exhibit band conduction in semiconducting bands with a finite energy gap at the Fermi level.

The solid line in Fig. 3(d) is the fitting result using Mott's variable range hopping (VRH) theory for 2D metals that have spatially localized metallic states [25,26], $\sigma_{2D} = \sigma_0 \exp(-(\Delta E/k_B T)^{1/3})$ with $\sigma_0 = 4.75\ \mu S/\square$ and $\Delta E = 2.74$ meV. This formula fits the experimental results well. Therefore, although the temperature range is limited only in 10–50 K, we adopt the VRH picture here. In this picture, the defective $\sqrt{7}\times\sqrt{3}$ surface has a constant density of states (DOS) at around the Fermi level, however, these states are spatially and strongly localized. Therefore, although the defective $\sqrt{7}\times\sqrt{3}$ surface still has metallic DOS, it exhibits a semiconducting temperature dependence due to the Anderson strong localization. The localization length ξ is estimated from the DOS at the Fermi surface $D_{2D} = m^*/\pi\hbar^2 = 4.6\ \mathrm{eV}^{-1}\,\mathrm{nm}^{-2}$ and the fitting result $\Delta E = 2.74$ meV using $\xi = \sqrt{3^3/\pi D_{2D}\Delta E}$, giving ξ to be 26 nm. The threshold defect density for the metallic-VRH conduction is roughly estimated to be 0.004–0.009 nm^{-2}.

In summary, we have succeeded in detecting metallic transport in the $\sqrt{7}\times\sqrt{3}$-In surface reconstruction down to 10 K. The $\sqrt{7}\times\sqrt{3}$ surface showed a resistivity smaller than the inverse of the minimum metallic conductivity and metallic temperature dependence of the resistivity. This system is a rare example of monatomic layers exhibiting metallic transport at cryogenic temperatures. By introducing defects, a metal-insulator transition occurred due to Anderson localization.

We thank F. Komori for fruitful discussions. This work was supported by Grants-In-Aid and the A3 Foresight Program from the Japan Society for the Promotion of Science.

*Shiro.Yamazaki@physik.uni-hamburg.de
Present address: Institute of Applied Physics and Microstructure Advanced Research Center, University of Hamburg, Jungiusstraße 11, D-20355 Hamburg, Germany.

[1] P. W. Anderson, Phys. Rev. **109**, 1492 (1958).
[2] S. Yamazaki *et al.*, Phys. Rev. B **79**, 085317 (2009).
[3] K. H. Lee, S. Cho, S. H. Park, A. J. Heeger, C.-W. Lee, and S.-H. Lee, Nature (London) **441**, 65 (2006).
[4] K. S. Novoselov *et al.*, Nature (London) **438**, 197 (2005).
[5] Y. Zhang *et al.*, Nature (London) **438**, 201 (2005).
[6] http://www.capres.com.
[7] T. Tanikawa *et al.*, e-J. Surf. Sci. Nanotechnol. **1**, 50 (2003).
[8] V. G. Lifshits, A. A. Saranin, and A. V. Zotov, *Surface Phases on Silicon* (John Wiley & Sons, West Sussex, 1994).
[9] J. Kraft, M. G. Ramsey, and F. P. Netzer, Phys. Rev. B **55**, 5384 (1997).
[10] T. Abukawa *et al.*, Surf. Sci. **325**, 33 (1995).
[11] H. W. Yeom *et al.*, Phys. Rev. Lett. **82**, 4898 (1999).
[12] E. Rotenberg *et al.*, Phys. Rev. Lett. **91**, 246404 (2003).
[13] H. M. Zhang, T. Balasubramanian, and R. I. G. Uhrberg, Phys. Rev. B **66**, 165402 (2002).
[14] A. V. Zotov *et al.*, Appl. Surf. Sci. **159–160**, 237 (2000).
[15] H. Lüth, *Surface and Interfaces of Solid Materials* (Springer-Verlag, Berlin, 1995).
[16] S. Hasegawa *et al.*, Prog. Surf. Sci. **60**, 89 (1999).
[17] S. Takeda *et al.*, Surf. Sci. **415**, 264 (1998).
[18] T. Tanikawa, Ph.D. thesis, Univ. Tokyo, 2003.
[19] T. Tanikawa *et al.*, Phys. Rev. Lett. **93**, 016801 (2004).
[20] A. F. Ioffe and A. R. Regel, Prog. Semicond. **4**, 237 (1960).
[21] G. D. Mahan, *Many-Particle Physics* (Kluwer Academic/Plenum, New York, 2000).
[22] E. W. Plummer *et al.*, Prog. Surf. Sci. **74**, 251 (2003).
[23] T. Zhang *et al.*, Nature Phys. **6**, 104 (2010).
[24] P. A. Lee and T. V. Ramakrishnan, Rev. Mod. Phys. **57**, 287 (1985).
[25] N. F. Mott, J. Non-Cryst. Solids **1**, 1 (1968).
[26] A. Bostwick *et al.*, Phys. Rev. Lett. **103**, 056404 (2009).